Compact cyclotron resonance high-power accelerator for electrons

S. V. Shchelkunov, X. Chang, and J. L. Hirshfield[*]

Particle Accelerator Research Foundation 291 Whitney Avenue, Suite 401,
New Haven, Connecticut 06511, USA

Exact numerical solutions for the single particle equations of motion have revealed conditions for highly nonlinear rapid acceleration near cyclotron resonance for electrons injected into a TE_{111}-rotating-mode cylindrical microwave cavity immersed in a uniform axial magnetic field. We dub this the eCRA interaction. Magnitudes of acceleration energy in eCRA are shown to exceed to a large degree the limits for the related cyclotron autoresonance acceleration (CARA) interaction, wherein autoresonance acceleration is sustained for traveling rotating TE_{11}-mode waves in a cylindrical waveguide. As with CARA, all injected electrons in an idealized eCRA enjoy equal energy gain without bunching. Injection of high currents that involve heavy beam loading allow acceleration in eCRA to multi-MeV levels for beams with average powers of hundreds of kW and rf-to-beam power efficiencies that exceed 80%. It is shown, to cite one example, that an effective acceleration gradient of over 90 MV/m can be sustained with a maximum cavity surface field of only 40 MV/m, when producing a 4.5 MeV, 300 kW average power electron beam, with an rf-to-beam efficiency of about 86%. In that example, the cavity operates at 2.856 GHz, and the cavity's average surface heating rate is 100 W/cm^2. Other examples are given for beams with over one MW levels of average power and energies up to about 20 MeV. This paper's goal is only to elucidate and give examples of the basic mechanism for the strongly nonlinear acceleration that is predicted to occur in eCRA, rather than to present a particular engineered design. Still, the predicted parameters for an idealized eCRA suggest that practical realizations could emerge to satisfy a range of needs for efficient, compact accelerators for industrial, commercial, and national security applications.

I. INTRODUCTION

Investigations continue, aimed towards development of compact, efficient, low-cost, high-power electron accelerators for scientific, national security, industrial and commercial applications. Typically, these accelerators are to produce beams with average powers of up to hundreds of kW and above, and particle energies of up to 10 MeV—a limit that is often imposed to minimize activation, neutron production and shielding mass. Applications for MW-level beam powers exist for remediation of polluted wastewater streams, flue gas and other effluents; neutralization of toxic solid wastes; and numerous industrial processes [1,2]. Lower power applications are in bremsstrahlung sources for sterilization of medical instruments and supplies, foodstuffs, and photonuclear reactions to produce radioisotopes [3], and for production of intense THz radiation [4].

[*]Corresponding author.
jay.hirshfield@yale.edu

A variety of industrial accelerators already exist that are designed to meet these needs [5]. But it may be that a practical realization of the electron cyclotron resonance accelerator (eCRA) based on the theory presented in this paper could be a competitive alternative to some of those machines.

A candidate suggested over 25 years ago for some of these applications is the cyclotron autoresonance accelerator (CARA) [6]. In CARA, a laminar continuous electron beam is injected along the axis of a TE_{11}-mode cylindrical waveguide that is immersed in an axial magnetic field. The waveguide is driven by exciting the two degenerate TE_{11} traveling-wave modes in quadrature to comprise a rotating traveling wave, with parameters tuned to satisfy the resonance condition,

$$\omega = \omega_c + k_z v_z, \qquad (1)$$

where ω is the wave's radian frequency; k_z is the wave's axial wave number; v_z is the axial velocity of the electrons, $\omega_c = eB/m\gamma$ is the relativistic cyclotron frequency for electrons with charge e and mass m in a static guide magnetic field B; and the relativistic energy factor is $\gamma = 1 + eV/mc^2$, with eV being the particle's kinetic

energy upon acceleration through a voltage V and mc^2 its rest energy. In addition to satisfaction of Eq. (1), the waveguide dispersion relation $\omega^2 = \omega_o^2 + k_z^2 c^2$ must also be satisfied, where ω_o is the cutoff frequency. Prominent properties of a CARA beam include its absence of bunching, since—except for phase—it has been shown that all electrons in an idealized beam enjoy equal energy gain and no phase focusing. The absence of bunching mitigates against space-charge issues—including instabilities—that arise with dense bunches in high-current beams. Further, a CARA beam is self-rastering, since the beam particles trace helices as they exit along a diverging guide magnetic field and thus will constitute a beam that automatically scans upon impacting a target.

A serious limitation of the CARA mechanism is its intrinsic upper energy limit, given by

$$\gamma_{\max} = \gamma_o + \left[\frac{\gamma_o^2 - 1}{1 - n^2}\right]^{1/2}, \tag{2}$$

where γ_o and $\gamma_{\max}$ are the initial and maximum relativistic energy factors. Here $n = ck_z/\omega = v_g/c$, with v_g the wave group velocity. This limit applies when autoresonance, which can be written $\gamma(1 - n\beta_z) = \text{const.}$ is satisfied throughout the acceleration, where $\beta_z = v_z/c$ is the particle's normalized axial velocity. Autoresonance can be satisfied during acceleration by either tapering the guide magnetic field, or by tapering the waveguide radius; the upper energy limit is the same for either option. For example, a 200 keV beam injected into a waveguide operating at a frequency just above cutoff for the TE_{11} mode $((0.293c/R))$, and then tapered up in radius by about 30% to just below cutoff for the next higher mode (TM_{01}), could not be accelerated to beyond 0.968 MeV, according to this formula. Here, R is the waveguide radius. As a consequence, CARA acquired the notorious reputation as a "gamma doubler," so despite its other attributes it has not found much acceptance in the accelerator community.

This paper describes an alternate concept for cyclotron resonance acceleration of electrons that employs a cylindrical cavity operating under conditions that do not conform to autoresonance. We have carried out detailed numerical solutions of the highly nonlinear equations that govern motion for electrons injected into a TE_{111}-mode cavity immersed in a strong axial magnetic field. The rf fields of the cavity are a superposition of two orthogonal modes excited in quadrature to comprise a rotating

standing-wave mode. In general, we find much higher upper energy limits than that given by Eq. (2). These limits arise when slippage in phase between the particle's momentum and the rf electric field moves from accelerating into decelerating ranges, or by particle interception on the cavity wall. We choose the moniker "eCRA" to label this interaction, dropping the A that signifies "auto," in CARA; and adding the prefix e to make clear that this interaction is not appropriate for acceleration of ions. It bears emphasis that this paper is only to elucidate the fundamental eCRA accelerator mechanism, and not to present any practical design for an actual accelerator, although some practical issues are touched upon. What is presented in the following sections should thus be viewed solely as an idealization.

This paper is organized as follows. Section II presents the governing equations and method used for numerical solution to determine beam dynamics. Section III includes graphical results that show the nature of particle orbits and energy limits during acceleration. Section IV describes the method for determining efficiency and gives some examples. Finally, Sec. V summarizes the results, points out their limitations, describes future directions toward practical realization of a demonstration eCRA, and suggests possible applications.

II. GOVERNING EQUATIONS AND THE MEANS FOR THEIR SOLUTION

In this section, we list the equations for the fields in the idealized eCRA TE_{111}-rotating-mode cylindrical cavity, and the single-particle equations of motion for electrons injected into the cavity. The cavity radius and height are R and L. A uniform static magnetic field B_o aligned along the cavity axis of symmetry (z axis) permeates the cavity and the space beyond. From solutions of the equations of motion, the power balance and rf-to-beam efficiency are developed and illustrated in Sec. IV. Those considerations assume—as will be shown—that there is no spatial bunching for the particles, so we have taken space charge forces and space charge perturbations of the vacuum fields to be negligible, even for high currents where, as in bunched-beam accelerators such as cyclotrons and linacs, these effects may be non-negligible.

The electric field components for the two (degenerate) linearly polarized TE_{111} modes (also labeled in some texts as H_{111} modes) are

$$E_z(r, \varphi, z, t) = 0 \tag{3}$$

$$E_r(r, \varphi, z, t) = \left\{ \begin{array}{c} E_{w,0} \\ E_{w,90} \end{array} \right\} W \frac{J_1(k_c r)}{k_c r} \left\{ \begin{array}{c} \sin(\varphi) \\ -\cos(\varphi) \end{array} \right\} \sin(\beta z) \left\{ \begin{array}{c} \cos(\omega t) \\ \sin(\omega t) \end{array} \right\} \quad \text{and} \tag{4}$$

$$E_\varphi(r, \varphi, z, t) = \left\{ \begin{array}{c} E_{w,0} \\ E_{w,90} \end{array} \right\} W J_1'(k_c r) \left\{ \begin{array}{c} \cos(\varphi) \\ \sin(\varphi) \end{array} \right\} \sin(\beta z) \left\{ \begin{array}{c} \cos(\omega t) \\ \sin(\omega t) \end{array} \right., \tag{5}$$

where $J_1(x)$ is the Bessel function of the first kind of order one, x_{11} is the first zero of $J_1'(x)$, $k_c = x_{11}/R$; $\beta = \pi/L$; $W = x_{11}/J_1(x_{11}) = 1.8411/0.58187 = 3.1642$ is a normalization factor; E_w is the maximum electric field amplitude on the cavity walls, with subscripts 0 and 90 designating their relative phases. The corresponding magnetic field components are

$$B_z(r, \varphi, z, t) = (k_c/\omega) \left\{ \begin{array}{c} E_{w,0} \\ E_{w,90} \end{array} \right\} W J_1(k_c r) \left\{ \begin{array}{c} \cos(\varphi) \\ \sin(\varphi) \end{array} \right\} \sin(\beta z) \left\{ \begin{array}{c} \sin(\omega t) \\ -\cos(\omega t) \end{array} \right., \tag{6}$$

$$B_r(r, \varphi, z, t) = (\beta/\omega) \left\{ \begin{array}{c} E_{w,0} \\ E_{w,90} \end{array} \right\} W J_1'(k_c r) \left\{ \begin{array}{c} \cos(\varphi) \\ \sin(\varphi) \end{array} \right\} \cos(\beta z) \left\{ \begin{array}{c} \sin(\omega t) \\ -\cos(\omega t) \end{array} \right., \quad \text{and} \tag{7}$$

$$B_\varphi(r, \varphi, z, t) = -(\beta/\omega) \left\{ \begin{array}{c} E_{w,0} \\ E_{w,90} \end{array} \right\} W [J_1(k_c r)/k_c r] \left\{ \begin{array}{c} \sin(\varphi) \\ \cos(\varphi) \end{array} \right\} \cos(\beta z) \left\{ \begin{array}{c} \sin(\omega t) \\ \cos(\omega t) \end{array} \right., \tag{8}$$

where $\omega = c \sqrt{k_c^2 + \beta^2}$.

We write out these equations in full, since the forms for rotating modes are not found in most literature sources, the phase factors are critical, and our normalization differs from convention. When $E_{w,0} = E_{w,90}$, the sum of both components are such that E_r, B_z, and B_r vary as $\sin(\varphi - \omega t)$, while E_φ and B_φ vary as $\cos(\varphi - \omega t)$: namely circular clockwise rotating polarization; otherwise the polarization is elliptical. Of course, these equations represent the fields in an idealized cylindrical cavity, free of coupling irises for the applied rf and apertures for entry and exit of the electron beam.

The single-particle equations of motion are

$$ds = c\,dt \tag{9}$$

$$\mathbf{p} = \gamma(\hat{\mathbf{e}}_x \beta_x + \hat{\mathbf{e}}_y \beta_y + \hat{\mathbf{e}}_z \beta_z) \tag{10}$$

$$\gamma = \sqrt{1 + \mathbf{p} \cdot \mathbf{p}} \tag{11}$$

$$\mathbf{r} = (\hat{\mathbf{e}}_x x + \hat{\mathbf{e}}_y y + \hat{\mathbf{e}}_z z) \tag{12}$$

$$d\mathbf{r}/ds = \mathbf{p}/\gamma \tag{13}$$

$$d\mathbf{p}/ds = -(e/mc^2)(\mathbf{E} + c\mathbf{p} \times \mathbf{B}/\gamma), \tag{14}$$

where dt is the time interval; (x, y, z) are the particle's Cartesian coordinates, $\mathbf{E}$ is the total electric field at the particle location, and $\mathbf{B}$ is the total magnetic field at the particle location, including both the rf and static components, the latter designated as $\mathbf{B}_o$.

The equations of motion are solved for each electron in PYTHON [7], using PYTHON modules NumPy [8] and SciPy [9]. Graphs are plotted ether using PYTHON MATPLOTLIB [10], or MS Excel [11]. A simple integration scheme is used, in which the time-step size is varied to confirm convergence. A tracking algorithm checks whether a particle has hit a wall or other obstacle, and freezes it at that location.

III. PARTICLE ORBITS AND ENERGY LIMITS

In this section, selected results are shown of numerical solutions to the above equations. Examples have been picked that show eCRA performance for single particles or finite-length uniform streams of particles injected along the cavity axis. The TE$_{111}$ cavities that are considered all resonate at 2.856 GHz, and have radii beginning just above the cutoff radius of 3.078 cm and up to 7.0 cm. Cavity dimensions and surface areas are listed in Table I.

It was found, depending on the rf-field strength (as characterized by E_w) and the magnitude of the guide magnetic field B_o, that electrons are accelerated, but can either reach and are transmitted through the end wall of the cavity, or can be reflected back. (The walls of the idealized cavity are taken to be transparent to electrons in our idealization.) Figure 1 shows examples of nonreflecting and reflecting orbits, for parameters listed in the caption.

TABLE I.   Cavity dimensions and surface areas for TE$_{111}$ cavities that resonate at 2.856 GHz.

Radius R (cm)	3.50	4.00	4.50	5.00	5.50	6.00	6.50	7.00
Length L (cm)	11.00	8.21	7.19	6.66	6.33	6.11	5.96	5.84
Surface area (cm^2)	318.9	306.9	330.5	366.2	408.9	456.6	508.8	564.9

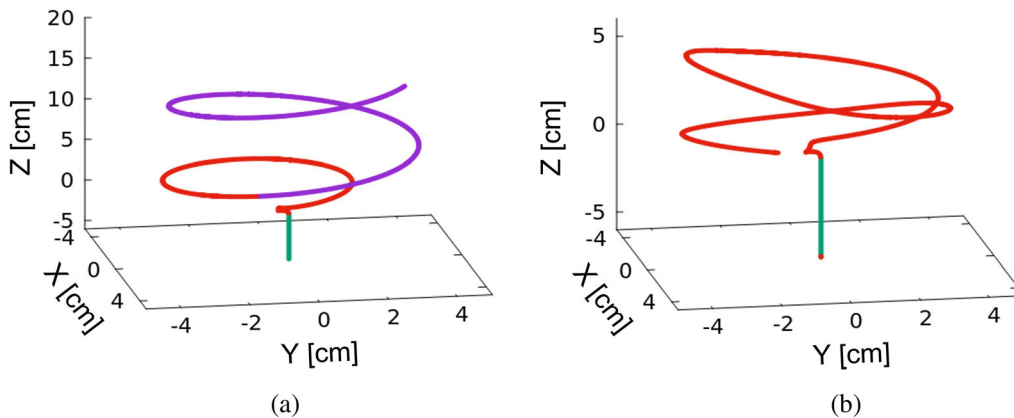(a)   (b)

FIG. 1.   Particle orbits within an eCRA cavity. Example (a) is for a cavity with radius $R = 6.0$ cm and length $L = 6.113$ cm, showing a nonreflecting orbit; while for (b), $R = 7.0$ cm and $L = 5.84$ cm, showing an orbit that reflects within the cavity. Both are for injected particle energies of 100 keV, and for $E_w = 100$ MV/m. In (a) the guide magnetic field $B_o = 0.914$ T, while in (b) $B_o = 0.650$ T. The electron trajectories are in green (before the cavity), red (in the cavity) and violet (after the cavity). Note that the orbit shown in (a) achieves full acceleration to 10.13 MeV in only about one turn.

Energy gain for a range of cavity fields E_w are shown in Fig. 2, as functions of axial distance along the cavity. These examples are for a cavity with $R = 6.0$ cm and $L = 6.113$ cm, with injected particles having energies of 100 keV. Other parameters are listed in Table II.

For the 100 MV/m case, for example, a 10.13 MeV gain in 6.113 cm corresponds to an acceleration gradient of 166 MeV/m. For typical linacs, the maximum E-field at the wall usually exceeds the acceleration gradient, whereas here the opposite is the case.

Electrons of identical energies and zero transverse momenta that enter the cavity on axis ($x = y = 0$) but at different times within an rf cycle will evolve identically in their energy gains, but will emerge from the cavity at different radii and different azimuthal angles. An example
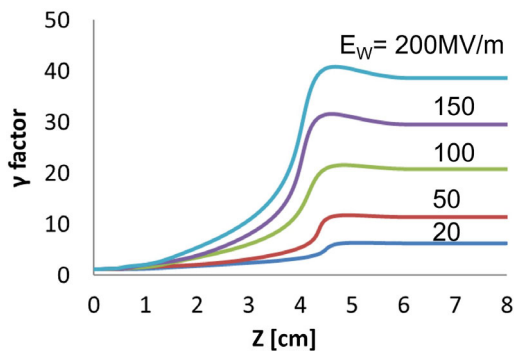

FIG. 2.   Increase in relativistic energy factor γ of nonreflected electrons in an eCRA cavity with $R = 6.0$ cm, and $L = 6.113$ cm, for the indicated values of maximum rf electric field at the wall E_w. The electrons enter at $x = y = z = 0$, with initial kinetic energy 100 keV. Energy gain is seen to be mainly in the ~3-cm central region of the cavity where the E-fields are strongest; but the nominal acceleration gradient values we cite are equal to the energy gain divided by the full cavity length. See Table II for other parameters.

of this is shown in Fig. 3(a), which is a projection on a transverse plane of the helical motion of a single accelerated particle orbiting on a circle whose center is offset from the cavity axis. This offset is caused by a small transverse $v \times B$ kick encountered as particles enter the cavity. This kick arises from the strong rf B-field on the inner cavity surface, so the azimuthal angle of this kick varies cyclically with the rf phase. This variation is illustrated another way in Fig. 3(b), which depicts the radial coordinate for a particle as a function of its distance z from the cavity entrance. The periodic variation of about 0.35 cm comes from the eccentric nature of the circular orbit, while the drop in radial coordinate near $z = 0$ is because the particle is still within the cavity and has thus received only partial acceleration. All particles exhibit the same behavior, except for their variation in azimuth angle. The imprint of such a beam on a fixed target normal to the axis is shown in Fig. 3(c). It is an accumulation of loci where particles in a continuous stream moving on offset helical orbits intersect the target. This superposition is centered on the axis. It shows the particles to be uniformly distributed in azimuth, and to lie on a circle at other target locations, so long as the axial field B_o remains constant. The uniform distribution of points in Fig. 3(c) confirms the absence of azimuthal bunching in the eCRA interaction; it should be understood to be fundamental, since the system

TABLE II.   Parameters for Fig. 2.

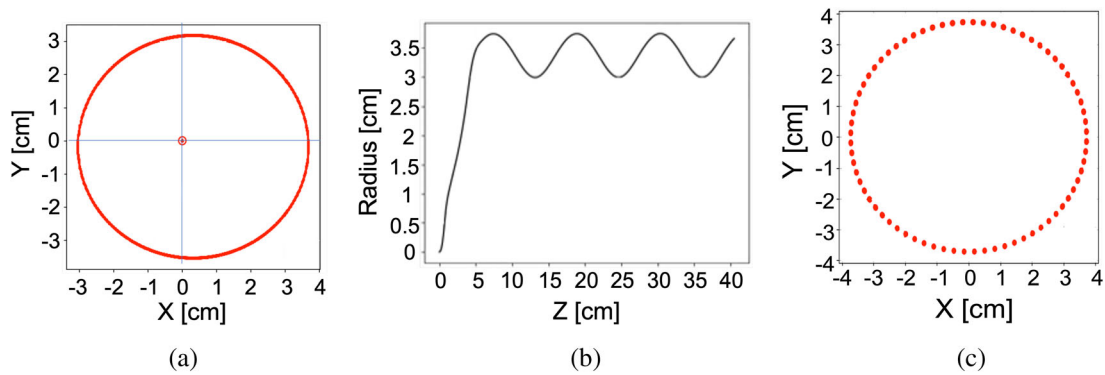| E_w (MV/m)	20	50	100	150	200
B_o (T)	0.331	0.535	0.914	1.297	1.656
Final electron energy (MeV)	2.68	5.31	10.13	14.59	19.25
Nominal acceleration gradient (MV/m)	43.8	86.9	165.7	238.7	314.9

FIG. 3. (a) Projection on a plane transverse to the cavity axis over one or more rf periods of the eccentric helical orbit of an accelerated particle. Note the 0.35 cm offset of this helix's axis from (0,0). (b) Plot of the radial coordinate of a particle along z showing the undulation from its initial radial kick that causes the offset of eccentric helical orbits. (c) Superposition over a full cycle of the loci of orbit intersections where particles intersect a target beyond the cavity. This shows how an eCRA beam is centered on (0,0), how it would scan and deposit its energy uniformly around a circle on a target, and how it remains unbunched.

we consider here has full azimuthal symmetry. But the radius of this uniform distribution will vary slightly with z as depicted in Fig. 3(b), since the proration of azimuthal and radial momenta varies slightly with z, even as all electrons have identical energies. That latter fact, plus the identical angular momenta of all electrons with respect to

their own axes, also shows that all electrons have equal longitudinal momentum; ergo no longitudinal bunching.

The variation in beam radius with z in this idealized model of eCRA may be of minor significance in applications where the precise beam location on a target is not of consequence. Still, it could pose a problem where
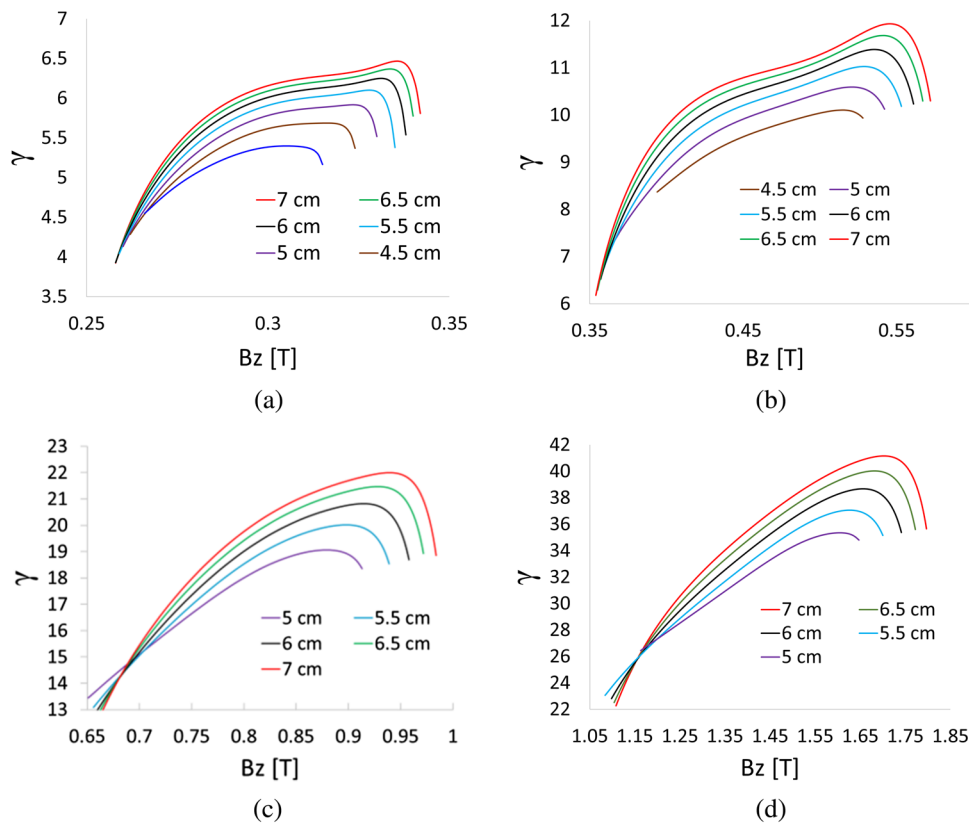

FIG. 4. Behavior of final values of γ vs B_o as electrons exit cavities of various radii, with curves labeled according to the cavity radius R in cm. (a) $E_w = 20\,MV/m$ (b) $E_w = 50\,MV/m$ (c) $E_w = 100\,MV/m$ (d) $E_w = 200\,MV/m$. Eneries of accelerated electrons in these examples are between about 2 and 20 MeV.
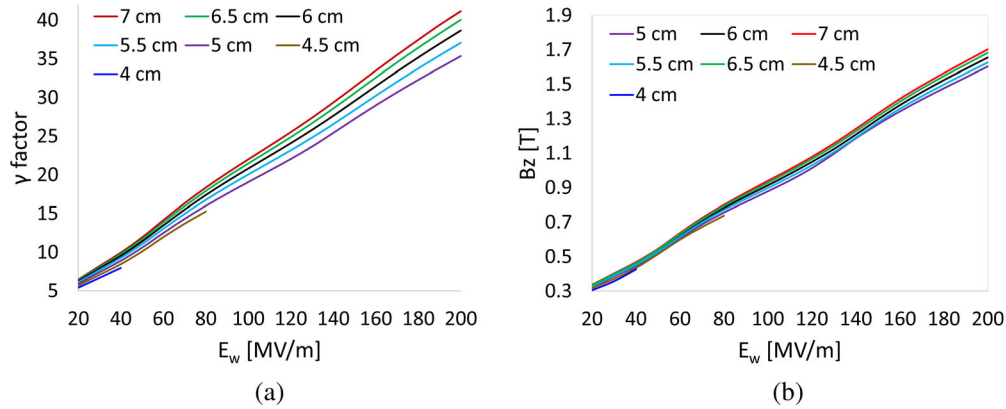
FIG. 5.   (a) Final maximum gamma factors vs E_w for various cavity radii; (b) corresponding values of B_o.

interaction of the beam with a circuit is intended, as in a THz source. But in reality the magnitude of the transverse kick may be minimized by design of the cavity's entrance aperture for the beam, since this can effect a reduction of the rf B-field near the entrance.

For each cavity radius and at given values of E_w, a range of values of B_o can be found where an electron will not be reflected as it is accelerated. This behavior was explored for values of E_w between 20 and 200 MV/m, with a step size of 10 MV/m. We also scanned for values of B_o with a step size of 10^{-3} T. A few examples are shown in Fig. 4, where we plot the final values of γ at the cavity exit versus B_o for the four indicated values of E_w. These considerations show that eCRA can evolve into an accelerator of widely varying beam energy, as can be achieved by adjustment of the rf power level and associated values of magnetic field B_o.

There is a value of B_o for which the gamma factor is maximized. If we plot these maxima, we obtain the family of curves shown in Fig. 5(a). The corresponding values of B_o are shown in Fig. 5(b).

Finally, we investigated the effect that nonuniformity in the B_o profile would have, and found that a relatively high nonuniformity can be tolerated without diminution in the acceleration. For example, a linear slope as high as 20% along the axis of a 6.113-cm long cavity showed only a minor change in energy gain. This can be understood, for although cyclotron resonance is indeed a factor in the acceleration mechanism, evidence that energy gain occurs in only a very few orbit turns suggests that the resonance is broad—and thus not sensitive to moderate B_o-field variations.

IV. EFFICIENCY

While rf-to-beam power efficiency may not be the primary consideration for some accelerators, it is clearly a dominant consideration for any accelerator that produces high average power beams; that is clearly the intended regime for the eCRA's that we consider in this paper. This section describes the method for determining eCRA

efficiency, even as we emphasize it to be an idealization. One assumption, as mentioned in Sec. II, is that space-charge fields and space-charge forces associated with a finite-current beam neither perturb the imposed rf fields nor the single-particle orbits as found in Sec. III. The plausibility of these assumptions arises from the fact that particles are not bunched in this interaction, thereby avoiding the strong localized fields associated with high-current bunched beams. Further, as also stated above, the cavity geometry used here is that of a perfect unpenetrated cylinder, free of beam and coupler apertures. Accordingly, it is to be expected that any practical realization of an eCRA is bound to have lower efficiency than found here. Still, it is important to show that—in principle—efficiency for the eCRA mechanism can be high; for otherwise there would be little justification for developing practical realizations if low efficiency were to have been predicted in advance.

The approach taken here begins by specifying the maximum local surface electric field E_w on the TE_{111} cavity wall, since this parameter is linked directly to the maximum acceleration itself, and since extensive rf breakdown studies offer guidance for determining field limits that ensure reliable operation [12]. When numerical results are cited here, they are for operation at 2.856 GHz, since at this frequency well-developed high-power rf sources, rf components and rf pulse compressors exist for near-term demonstrations of eCRA. Still, future studies could show that a lower frequency, for example 915 or 650 MHz, might be preferable, since Ohmic wall losses would be lower, orbit paths in the cavities would be longer and—especially for cw operation—where available low-cost high-power efficient magnetrons are available.

Efficiency η is defined here as

$$\eta = \frac{\bar{P}_b}{\bar{P}_b + \bar{P}_w},\tag{15}$$

where the bars indicate that the electron beam and cavity wall powers are time-averaged values. The time-averaged beam power is given by $\bar{P}_b = I_{peak}V_{peak}\Delta$ where the

subscripts denote peak values of beam current I and beam voltage V, to characterize parameters for pulsed beams. The duty factor, or fraction of time the beam is on, is denoted by Δ. The time-averaged cavity wall power is determined from the relationship $\bar{P}_w = \omega \bar{U}/Q$, where $\bar{U} = U\Delta$ is the time-averaged stored energy in the cavity and Q is the cavity quality factor. There is a limit p_{lim} to the areal average power dissipation that the cavity can in practice sustain; this in turn sets $\bar{P}_w \leq A p_{lim}$, where A is the effective cavity surface area. As a given value of E_w (and thus P_w) is required to effect acceleration to a desired level, this in turn sets the duty factor to be $\Delta = A p_{lim}/P_w$.

It is from E_w that we shall determine U, as given in a standing-wave cavity by

$$U = U_e + U_h = \frac{\varepsilon}{2} \iiint E^2 dV + \frac{\mu}{2} \iiint H^2 dV$$

$$= [\cos(\omega t)]^2 \frac{\varepsilon}{2} \int_V E^2 dV + [\sin(\omega t)]^2 \frac{\mu}{2} \int_V H^2 \, dV. \quad (16)$$

However, when only one mode (or the two degenerate modes) is excited in a cavity, one has

$$\frac{\mu}{2} \int_V H^2 \, dV = \frac{\varepsilon}{2} \int_V E^2 \, dV. \quad (17)$$

So stored energy, in the absence of losses, does not change with time:

$$U = [\cos^2(\omega t) + \sin^2(\omega t)] \frac{\varepsilon}{2} \int_V E^2 dV = \frac{\varepsilon}{2} \int_V E^2 dV. \quad (18)$$

Thus,

$$\int_V E^2 \, dV = \left\{ \begin{matrix} E_{w,0}^2 \\ E_{w,90}^2 \end{matrix} \right\} W^2 \int_0^L \sin^2(\beta z) dz \int_0^{2\pi} d\varphi \left(\begin{matrix} \sin^2(\varphi) \\ \cos^2(\varphi) \end{matrix} \right) \int_0^a r dr \left[\frac{J_1(k_c r)}{k_c r} \right]^2$$

$$+ \left\{ \begin{matrix} E_{w,0}^2 \\ E_{w,90}^2 \end{matrix} \right\} W^2 \int_0^L \sin^2(\beta z) dz \int_0^{2\pi} d\varphi \left(\begin{matrix} \cos^2(\varphi) \\ \sin^2(\varphi) \end{matrix} \right) \int_0^a r dr \, [J_1'(k_c r)]^2. \quad (19)$$

This leads to the stored energy in each of the linearly polarized modes to be

$$\left\{ \begin{matrix} U_0 \\ U_{90} \end{matrix} \right\} = \left\{ \begin{matrix} E_{w,0}^2 \\ E_{w,90}^2 \end{matrix} \right\} \pi a^2 L \frac{\varepsilon}{4} \frac{\int_0^{\chi_{11}} x dx [(\frac{J_1(x)}{x})^2 + [J_1'(x)]^2]}{J_1^2(\chi_{11})}. \quad (20)$$

Numerical computation finds that

$$\frac{\varepsilon}{4} \frac{\int_0^{\chi_{11}} x dx [(\frac{J_1(x)}{x})^2 + [J_1'(x)]^2]}{J_1^2(\chi_{11})} = 2.645 \times 10^{-12} \text{ Farads/m.} \quad (21)$$

So the stored energy for each linear polarization becomes

$$\left\{ \begin{matrix} U_0 \\ U_{90} \end{matrix} \right\} = 2.645 \times 10^{-12} \, \pi a^2 L \left\{ \begin{matrix} E_{w,0}^2 \\ E_{w,90}^2 \end{matrix} \right\} \text{ Joules.} \quad (22)$$

For calculations that follow, the sum of both values given by Eq. (22) are used, since eCRA requires two TE_{111} modes excited in quadrature, each with the same amplitude.

The quality factor Q for the TE_{111} mode is calculated from the formula given in Ref. [13]

$$Q \frac{\delta}{\lambda} = \frac{[1 - (\frac{1}{x_{11}})^2][x_{11}^2 + (\pi D/2L)^2]^{3/2}}{2\pi[x_{11}^2 + (\pi/2)^2(D/L)^3 + (1 - \frac{D}{L})(\frac{\pi D}{2Lx_{11}})^2]}, \quad (23)$$

where δ is the skin depth, $\lambda = 0.105$ m is the wavelength, and $D = 2R$. Figure 6 shows a curve of Q versus cavity
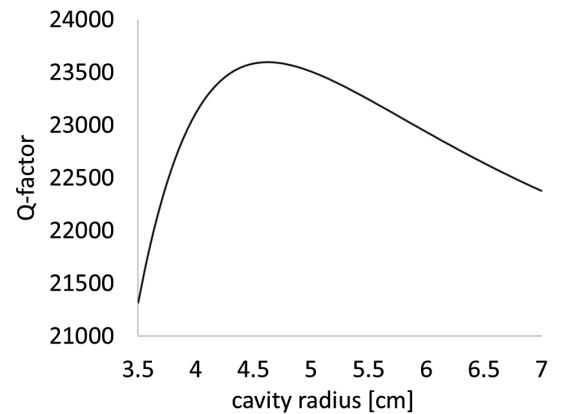

FIG. 6. Quality factor vs radius for TE_{111} copper cavities resonant at 2.856 GHz. Realistic cavities, with beam and coupling apertures, will have lower values.
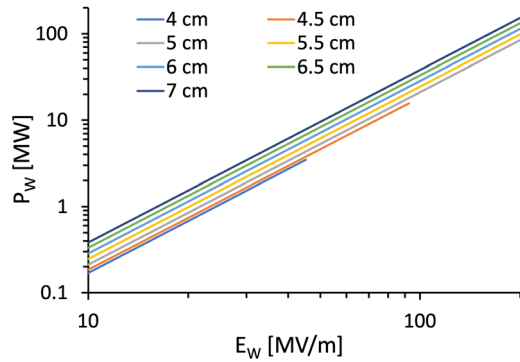
FIG. 7. Values of peak rf power P_w needed to sustain the given values of E_w, for a range of cavity radii.

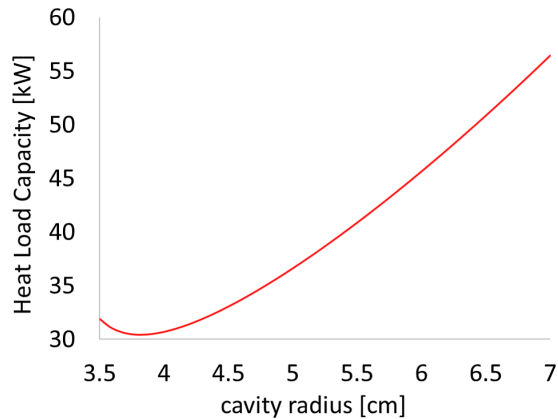
FIG. 8. Maximum average power that can be dissipated on TE_{111} cavity walls versus radius of a 2.856 GHz cavity, when the average areal power is 100 W/cm^2.

radius for TE_{111} cavities whose lengths are chosen for resonance at 2.856 GHz, and for copper walls with a conductivity of 5.87×10^7 S/m. These Q values could be increased by a factor of 2 or more by employing cryogenic cooling to 77 °K [12].
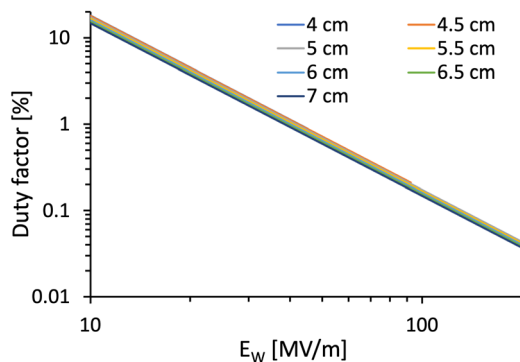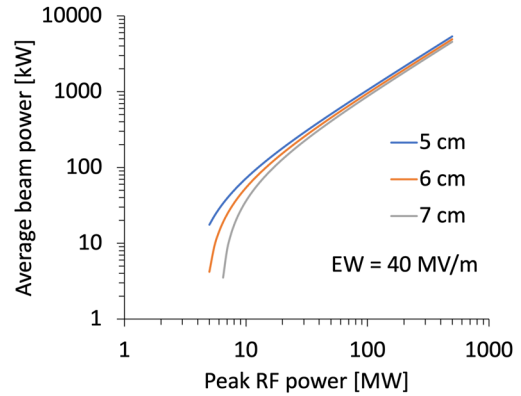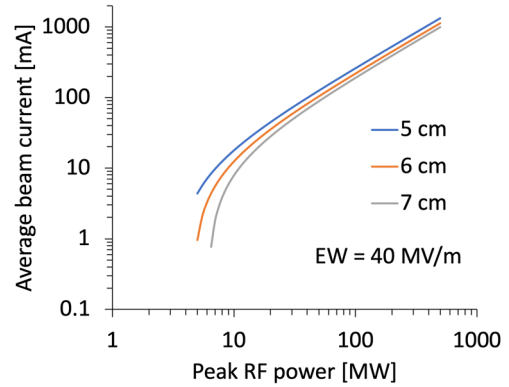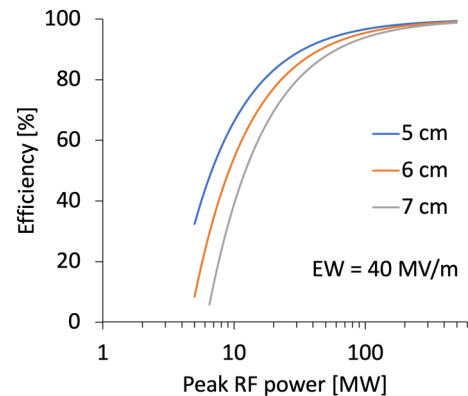

FIG. 9. Maximum duty factors Δ that are consistent with the wall heat load values in Fig. 8.

FIG. 10. (a) Average beam power, (b) average beam current, and (c) rf-to-beam efficiency; for eCRA's at 2.856 GHz operating with peak wall fields of 40 MV/m, for three cavity radii. For these cavities, accelerations up to 4.03, 4.36, and 4.58 MeV, respectively, are predicted.

These Q values, together with values of peak stored energy U as determined from Eq. (22) allow calculation of the peak rf power P_{wall} needed to sustain given values of E_w, for a range of cavity radii. Results are in Fig. 7. Two curves stop short where particle reflections occurred.

Finally, as described above, the duty factor Δ is determined approximately by dividing the peak wall power P_w by the surface area of the cavity $2\pi R(R + L)$ to find the
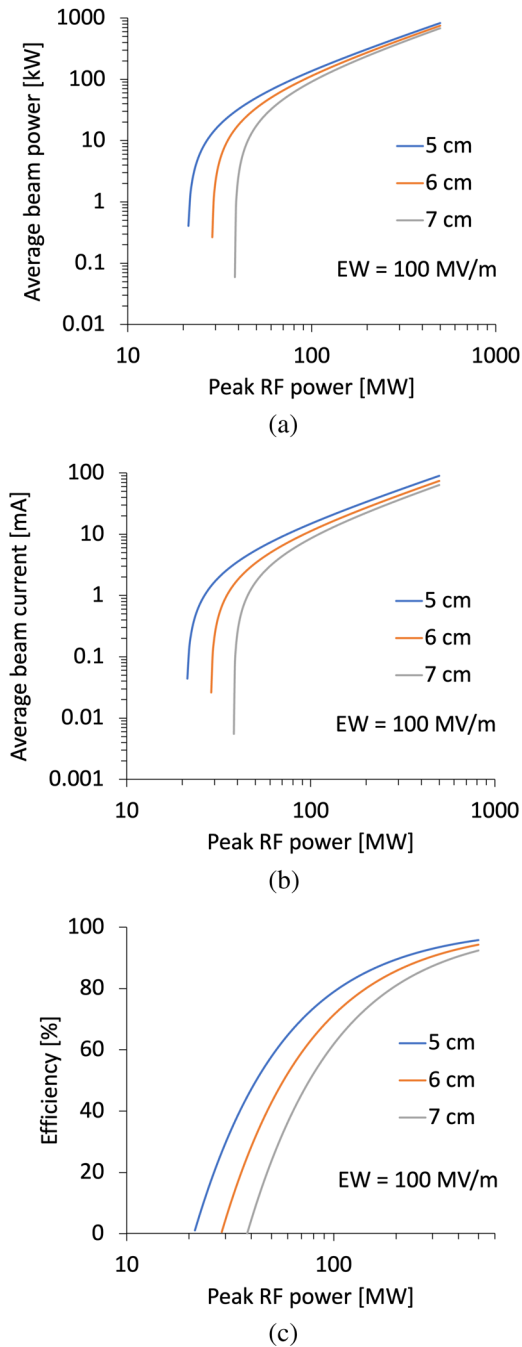
FIG. 11. Similar to Fig. 10, except for peak wall fields of 100 MV/m. For these cavities, accelerations up to 9.7, 10.2, and 10.7 MeV, respectively, are predicted.

surface-averaged peak areal power p_{av} that must be dissipated on the wall. For an acceptable value of p_{av}, which we denote as p_{ok}, it then follows that $\Delta = p_{ok}/p_{av}$. In the numerical evaluations that follow, we have taken $p_{ok} = 100$ W/cm^2. Figure 8 shows the maximum total wall power $\bar{P}_w$ that can be dissipated for this value of p_{ok}, while Fig. 9 shows the resulting duty factors.

It is important to stress that, while the discussion so far does not take into account beam loading, values of the duty

factor need not change when a beam is introduced. That is because the rf power dissipated on the cavity walls is determined directly by E_w, and its value can be held constant when a beam is introduced by adding additional rf drive power just sufficient to supply the beam, on top of the power lost to the walls. Use of this common procedure is illustrated here for the specific example of $E_{wall} = 40$ MV/m. Beam dynamics calculations described in Sec. III show for cavities with radii of 5.0, 6.0 and 7.0 cm that beams can be accelerated to final energies up to 4.03, 4.36, and 4.58 MeV, respectively. Figures 10(a)–10(c) show maximum values of average beam power, average beam current, and rf-to-beam efficiency for these three cavity radii. These plots illustrate the theoretical capabilities of eCRA for highly efficient production of MW-level beams, while limiting cavity wall heating to 100 W/cm^2. Further examples for beam energies above 10 MeV are shown in Fig. 11, where $E_{wall} = 100$ MV/m.

Figures 10 and 11 show examples where MW- and multi-MW beams at energies between 4.03 and 10.7 MeV could be produced efficiently in highly compact cavities operating at 2856 MHz. The rf field levels taken for the cavities, with wall fields and average areal powers that do not exceed 100 MV/m and 100 W/cm^2 are well within ranges that are reliably sustained [12].

V. DISCUSSION

Exact numerical solutions for the single particle equations of motion have revealed conditions for strong acceleration near cyclotron resonance for electrons injected into a TE$_{111}$-rotating-mode cylindrical cavity immersed in a strong axial magnetic field. The moniker eCRA is designated for this compact accelerator. Acceleration levels without bunching are shown to exceed to a large degree the limits for the CARA interaction, wherein autoresonance acceleration is sustained for traveling rotating TE$_{11}$-mode waves in a cylindrical waveguide. High current beams with accompanying heavy beam loading are shown to experience acceleration in eCRA to multi-MeV levels for beams with average powers of hundreds of kW and efficiencies that exceed 80%. It is shown, to cite one example (see Figs. 10), that an effective acceleration gradient of over 90 MV/m (4.5 MeV gain over 5.0 cm) can be sustained with a maximum cavity surface field of only 40 MV/m, when producing a 4.5 MeV, 300 kW average power electron beam, with an rf-to-beam efficiency of about 86%. In this example, the cavity operates at 2.856 GHz, the peak rf power level is 30 MW, and the average cavity surface heating rate is 100 W/cm^2. This accelerating cavity is remarkably compact, with a radius and length of each only about 6 cm. Other examples are shown for beams with over one MW level of average power and energies up to about 20 MeV. A given eCRA cavity is shown to allow wide variation in the accelerated beam energy by changing the rf power level and external magnetic field.

Calculations of beam dynamics in eCRA presented here are based on the single-particle equations of motion in the vacuum fields of an idealized TE_{111} cylindrical microwave cavity. We believe that these results are realistic in theory for validating the acceleration mechanism itself. That belief assumes that space-charge fields and forces will alter the results to but a small degree, since the beams are not bunched. Thus, one avoids strong field distortions of the cavity fields and beam stability issues that can be associated with tight bunching. Obviously, this assumption needs to be tested using simulation codes that take space charge effects into account. Another feature that must be refined is to analyze beam dynamics in a realistic cavity that includes apertures for beam entry and exit, and for rf couplers. Further, the realistic cavity design must include provision for a beam output window. However, in cases where the maximum radial beam excursion is less than the TE_{11}-mode cutoff radius (3.078 cm at 2.856 GHz), a beyond-cutoff pipe can be used to define the cavity field boundary, and thus an actual cavity window might not be required to contain the rf fields.

It should be stressed that the objective of this paper is not to present a conceptual design for an actual accelerator structure, but rather to elucidate the basic eCRA acceleration mechanism; namely rapid acceleration in a cavity near cyclotron resonance of high current electron beams to multi-MeV levels with high efficiency. Once the validity of this mechanism is confirmed with design codes that take space charge and realistic cavity geometry into account, specific applications for eCRA can be addressed. Such applications could be to supply the MW-level powers needed to generate electron or x-ray beams for remediation of wastewater streams, flue gases, and other effluents; and neutralization of toxic solid wastes. Lower power applications could be for beams to generate bremsstrahlung for photonuclear reactions to produce radioisotopes, for sterilization of medical instruments and supplies, and for production of intense THz radiation.

———

[1] Basic research needs workshop on compact accelerators for security and medicine: Tools for the 21st century, 2019; Michael Fazio, chair; Office of Science, U.S. Department of Energy.

[2] *Workshop on Energy and Environmental Applications of Accelerators, Argonne*, edited by S. Henderson and T. Waite (US Department of Energy, Washington, 2015), https://science.osti.gov/~/media/hep/pdf/accelerator-rd-stewardship/Energy_Environment_Report_Final.pdf.

[3] D. A. Rotsch *et al.*, Production of medical isotopes with electron linacs, in *Proceedings of NAPAC2016, Chicago, IL* (JACoW, Geneva, Switzerland, 2016), THB2I002.

[4] J. H. Booske *et al.*, Vacuum electronic high power terahertz sources, IEEE Trans. Terahertz Sci. Technol. **1**, 54 (2011).

[5] G. Burt, *Applications of Accelerators: Industrial Applications of Particle Beams* (The Cockcroft Institute, Lancaster University, Lancaster, 2016). See also https://www.cockcroft.ac.uk/wp-content/uploads/2016/07/Applications_1.pdf.

[6] B. Hafizi, P. Sprangle, and J. L. Hirshfield, Electron beam quality in a cyclotron autoresonance accelerator, Phys. Rev. E **50**, 3077 (1994); J. L. Hirshfield and C. B. Wang, Energy limit in cyclotron autoresonance acceleration, Phys. Rev. E **51**, 2446 (1995); M. A. LaPointe, R. B. Yoder, C. B. Wang, A. K. Ganguly, and J. L. Hirshfield, Experimental Demonstration of High-Efficiency Cyclotron Autoresonance Acceleration, Phys. Rev. Lett. **76**, 2718 (1996); J. L. Hirshfield, M. A. LaPointe, A. K. Ganguly, R. B. Yoder, and C. B. Wang, Multimegawatt cyclotron autoresonance accelerator, Phys. Plasmas **3**, 2163 (1996); Y. Jiang, S. V. Shchelkunov, and J. L. Hirshfield, Cyclotron autoresonance accelerator for environmental applications, Proc. AIP Conf. **1812**, 060003 (2017); Y. T. Yuan, K. J. Fan, and Y. Jiang, Cylindrical cavity design and particle-tracking simulation in cyclotron autoresonance accelerator, J. Phys. Conf. Ser. **1350**, 012064 (2019).

[7] https://www.python.org/.

[8] https://numpy.org/.

[9] https://www.scipy.org/.

[10] https://matplotlib.org/.

[11] https://www.microsoft.com/en-us/microsoft-365/excel.

[12] A. D. Cahill, J. B. Rosenzweig, V. A. Dolgashev, S. G. Tantawi, and S. Weathersby, High gradient experiments with X-band cryogenic copper accelerating cavities, Phys. Rev. Accel. Beams **21**, 102002 (2018), and references therein.

[13] *Technique of Microwave Measurements*, edited by C. G. Montgomery (McGraw-Hill, New York, 1947), p. 300.